Toxicity Mechanisms in *Escherichia coli* Vary for Silver Nanoparticles and Differ from Ionic Silver

Angela Ivask,[†,‡,§] Amro ElBadawy,[⊥] Chitrada Kaweeteerawat,[†,‡] David Boren,[†,¶] Heidi Fischer,[†,¶] Zhaoxia Ji,[†,‡] Chong Hyun Chang,[†,‡] Rong Liu,[†,‡] Thabet Tolaymat,[∥] Donatello Telesca,[†,¶] Jeffrey I. Zink,[†,‡,#] Yoram Cohen,[†,‡,△] Patricia Ann Holden,[†,▼] and Hilary A. Godwin[†,‡,▽,▲,*]

[†]University of California Center for Environmental Implications of Nanotechnology and [‡]California NanoSystems Institute, University of California, Los Angeles, California 90095, United States, [§]Laboratory of Environmental Toxicology, National Institute of Chemical Physics and Biophysics, 12618 Tallinn, Estonia, [⊥]Department of Environmental Engineering, University of Cincinnati, Cincinnati, Ohio 45221, United States, [∥]Office of Research and Development, U.S. Environmental Protection Agency, Cincinnati, Ohio 45268, United States, [¶]Department of Biostatistics, UCLA Fielding School of Public Health, [#]Department of Chemistry and Biochemistry, and [△]Department of Chemical and Biomedical Engineering, University of California, Los Angeles, California 90095, United States, and [▼]Bren School of Environmental Science & Management, and Earth Research Institute, [▽]Department of Environmental Health Sciences, UCLA Fielding School of Public Health, and [▲]Institute of the Environment and Sustainability, University of California, Los Angeles, California 90095, United States

ABSTRACT

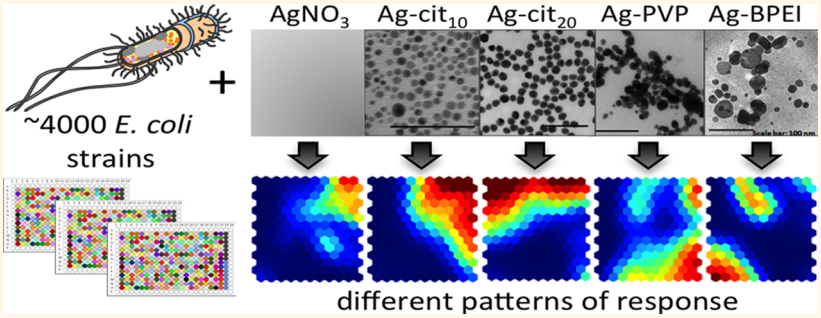

Silver nanoparticles (Ag NPs) are commonly added to various consumer products and materials to impair bacterial growth. Recent studies suggested that the primary mechanism of antibacterial action of silver nanoparticles is release of silver ion (Ag^+) and that particle-specific activity of silver nanoparticles is negligible. Here, we used a genome-wide library of *Escherichia coli* consisting of ~4000 single gene deletion mutants to elucidate which physiological pathways are involved in how *E. coli* responds to different Ag NPs. The nanoparticles studied herein varied in both size and surface charge. $AgNO_3$ was used as a control for soluble silver ions. Within a series of differently sized citrate-coated Ag NPs, smaller size resulted in higher Ag ion dissolution and toxicity. Nanoparticles functionalized with cationic, branched polyethylene imine (BPEI) exhibited equal toxicity with $AgNO_3$. When we used a genome-wide approach to investigate the pathways involved in the response of *E. coli* to different toxicants, we found that only one of the particles (Ag-cit_{10}) exhibited a pattern of response that was statistically similar to that of silver ion. By contrast, the pathways involved in *E. coli* response to Ag-BPEI particles were more similar to those observed for another cationic nanoparticle that did not contain Ag. Overall, we found that the pathways involved in bacterial responses to Ag nanoparticles are highly dependent on physicochemical properties of the nanoparticles, particularly the surface characteristics. These results have important implications for the regulation and testing of silver nanoparticles.

KEYWORDS: silver · nanoparticle · nanotoxicology · high-throughput screening · toxicology · bacteria · ecotoxicology

Colloidal silver, including formulations now known to contain silver nanoparticles (Ag NPs), has been used commercially for almost 100 years, typically as a biocide. However, registration of biocidal silver and nanosilver products has increased dramatically over the last 10 years,[1] most likely as a result of improved capabilities in nanoscience and engineering that allow Ag NPs to be formulated to confer increased durability and/or sustained antibacterial action, even under harsh environmental conditions.[2,3] As is the case for many other types of nanoparticles, a controversy has arisen about whether the Ag NPs should be subjected to increased regulatory scrutiny compared to macroscale or "bulk" silver.

* Address correspondence to hgodwin@ucla.edu.

Received for review August 22, 2013 and accepted December 16, 2013.

Published online December 16, 2013
10.1021/nn4044047

TABLE 1. Selected Characteristics of Nanomaterials Used in This Study

	primary size (nm)	ζ-potential in	hydrodynamic diameter	hydrodynamic diameter in bacterial growth media[b] (nm)	
	as prepared	DI water (mV)	in DI water (nm)[a]	0 h	24 h
			A. Ag NPs with variable primary size but similar surface properties		
Ag-cit$_{10}$	9.1 ± 4.2	−26.3 ± 2.6	17.0 ± 6.0	25.5 ± 8.2	32 ± 1
Ag-cit$_{20}$	19.1 ± 6.0	−33.8 ± 2.2	41.0 ± 19	45.0 ± 18	48 ± 4
Ag-cit$_{40}$	43.5 ± 12	−36.9 ± 1.8	65.5 ± 35	66.5 ± 25	73 ± 6
			B. Ag NPs with variable surface coating		
Ag-PVP	17.9 ± 7.0	−10.7 ± 1.8	85.5 ± 70	167.8 ± 85	166 ± 86
Ag-BPEI	23.3 ± 15	+33.3 ± 1.5	78.5 ± 42	85.5 ± 52	87 ± 41

[a] Based on intensity measurements. [b] LB media with 5% FBS.

Indeed, Ag NPs have been demonstrated to exhibit toxic effects in plants and bacteria at environmentally relevant concentrations.[4] The EPA's current position, based on the recommendations of an independent peer-reviewed scientific panel,[5] is that silver nanomaterials should be evaluated on a case-by-case basis.[6] This recommendation was based on the conclusion made by the panel that effects of nanosilver are dependent upon their physicochemical properties,[5] which in turn was based on a number of reports in the literature that demonstrated a correlation between toxicity of Ag NPs and their size, shape, and/or surface properties;[7−9] several studies since the time that the panel met have also supported this conclusion.[10−12] Although several authors have argued that dissolution of Ag ions from Ag nanoparticles (and the corresponding toxicity of Ag^+) is the main mechanism of the toxicity for Ag NPs,[2,13−17] some biological effects, including formation of reactive oxygen species (ROS)[13,18] and extensive membrane damage,[19−21] have been observed more severely for Ag NPs than for ionic Ag^+.[2,13−15] Recently, Alvarez and co-workers have argued that the physicochemical properties of Ag NPs influence the *magnitude* of their toxicity primarily because these properties alter the degree of dissolution and delivery of silver ions.[22] One of the reasons that this controversy has persisted is because most prior reports have typically focused on one or a few basic toxicological end points (*e.g.*, bacterial growth or generation of reactive oxygen species) and/or on a limited number and type of Ag NPs. Whether the physicochemical properties of Ag NPs also influence the *mechanisms* of toxicity has not been systematically explored for a broad range of different types of Ag NPs. To address this issue, mechanism-independent studies are needed to determine whether the physicochemical properties of Ag NPs influence how organisms respond to the particles and whether these responses are the same as or different from those observed for Ag^+. We recently reported the application of a genome-wide toxicity assay in the bacterium *E. coli* that allows the pathways by which the organism responds to nanoparticles to be determined.[23] This approach is ideally suited for addressing the question of whether Ag NPs exhibit particle-specific toxicity. In this experiment, a library of nonessential single gene deletion strains of *E. coli*[24] is screened to determine their fitness in the presence of a toxicant compared to the parent strain. Similar approaches have been used to study the mechanisms of action of a wide range of antimicrobial agents, including nanoparticles, in *E. coli*[25−28] and to elucidate the mechanisms by which both *E. coli* and *Saccharomyces cerevisiae* respond to different environmental stressors.[27,29,30] Unlike most toxicological assays, which test for the presence or absence of a particular end point (and hence mechanism or pathway), this high-throughput screening approach simultaneously reveals *all* statistically significant toxicological pathways and allows researchers to uncover previously unanticipated mechanisms. Here, we report the application of this approach to the investigation of a diverse series of Ag NPs of different sizes and surface coatings/charge.

RESULTS AND DISCUSSION

Ag Nanoparticles Varied in Their Size and Surface Properties. The silver nanoparticles studied herein varied in their primary size and surface coating. A series of three Ag NPs with the same shape and surface coating but different primary sizes were examined (Table 1). All three of these Ag NPs were spherical (Figure S1 in the Supporting Information) and had a negative ζ-potential (Table 1) due to the citrate that was used as stabilizing and coating material in the synthesis process. The as-prepared citrate Ag NPs had primary sizes of 9 nm (Ag-cit$_{10}$), 19 nm (Ag-cit$_{20}$), and 43.5 nm (Ag-cit$_{40}$) (Table 1). In addition, we investigated the properties of two additional types of Ag NPs, where polyvinylpyrrolidone (PVP; ζ-potential −10.7 mV) and branched polyethyleneimine (BPEI; ζ-potential +33.3 mV) were used as surface stabilizing agents for Ag NPs (Table 1; Figure S1 in the Supporting Information).

When dispersed in DI water, the hydrodynamic diameter of all the nanoparticles increased compared to their primary size, but the average diameter of Ag

TABLE 2. Dissolution, Bioavailability, and Bacterial Toxicity of Ag Nanomaterials

	in DI water		in bacterial growth media				
	Abs max (nm)[a]	% dissolved Ag[a]	Abs max (nm)[a]	% dissolved Ag[a]	% intracellular (bioavailable)[b] Ag^+ in bacterial growth media	IC_{50} (mg Ag/L)[c]	IC_{10} (mg Ag/L)[c]
Ag-cit_{10}	390	3.5	404	7	23.8	6.4	1.8
Ag-cit_{20}	404	3.7	408	5.7	7.1	15.7	8.0
Ag-cit_{40}	412	4.2	420	4.7	4.3	40.9	18.5
Ag-PVP	402	5.0	406	4.4	38	5.5	3.8
Ag-BPEI	420	6.2	426	26.9	110	2.2	1.4
$AgNO_3$		100		100	100	2.0	0.7

[a] Dissolved Ag was calculated from the difference in UV−vis spectrum (area under the curve, see Figure S2 in Supporting Information) of Ag NPs (12.5 mg Ag/mL) at 0 and 24 h. For the purposes of this analysis, data were normalized to $AgNO_3$ (*i.e.*, $AgNO_3$) and considered to be "100% dissolved" even though Ag^+ clearly undergoes additional speciation in complex media (*e.g.*, Ag^+ interacts with Cl^-). This normalization was based on the assumption that further speciation of Ag^+ would be the same for any silver ions generated from the particles studied as that of silver ions generated from $AgNO_3$. [b] Intracellular bioavailable Ag from Ag NPs was calculated from the induction of Ag biosensor by the Ag NPs. $AgNO_3$ was considered 100% bioavailable for the given test conditions; induction results are shown in Figure S3 in the Supporting Information. [c] The 24 h IC_{50} and IC_{10} values for BW25113(pACYC117), the parent strain of the library of gene deletion strains in growth inhibition assay.

NPs remained under 100 nm (Table 1) in all cases. When the particles were dispersed in bacterial growth (LB) media, their hydrodynamic diameter increased even further (Table 1). This was most likely due to proteins attaching on the surface of Ag NPs and coating the particles.[31] Despite some aggregation in LB media, the average size of the NP agglomerates remained below 200 nm under these conditions (Table 1) and remained stable for at least 24 h, which was the time period used for the toxicity studies.

Dissolution and Bioavailability Can Be Used To Predict the Magnitude of Antibacterial Activity of Different Ag Nanoparticles Compared to That of Ionic Ag^+ ($AgNO_3$). Because silver ions released upon dissolution of Ag nanoparticles have been proposed to be the primary contributor to the antibacterial activity of Ag NPs,[2,13,14,22] we performed toxicity and dissolution tests in parallel. The dissolution of the Ag NPs was analyzed using UV−vis absorption spectroscopy (Table 2 and Figure S2 in the Supporting Information), which is particularly useful because the surface plasmon resonance of Ag NPs in solution allows both the amount of NPs in solution (*via* the absorption) and the average size and size distribution of the particles in solution (*via* the wavelength corresponding to the absorption maximum and peak width) to be assessed.[32] According to UV−vis spectra, 3−7% of Ag NPs were dissolved in DI water while the dissolution of Ag NPs in LB media was generally higher (4−27%). Very similar results were obtained using atomic absorption spectroscopy (Table S1 in the Supporting Information) for all of the particles except Ag-cit_{10}. In the case of Ag-cit_{10}, the nanoparticles are too small to be effectively separated from solution using centrifugation. As a result, the AAS values for the percent of dissolved silver for Ag-cit_{10} using the atomic absorption spectroscopy method (which relies upon centrifugation for separation) were anomalously high (see Table S1 in the Supporting Information). Therefore, the values obtained for the percent dissolution for all of the species using the UV−vis method (which does not rely upon centrifugation) was considered to be more reliable and was used for the purposes of normalizing the data reported in the article.

Higher dissolution of NPs in media rich in organic compounds compared to that observed in blank water has been reported previously not only for Ag NPs[33] but also for CuO[34] and ZnO[35] nanoparticles. The reason that nanoparticles dissolve more completely in organic-rich media could be due to formation of metal ion organic complexes. Recent studies have shown that Ag NP dissolution can also be enhanced in chloride- or sulfide-rich media.[36] In LB media, a correlation between the primary size of the citrate-coated particles and their dissolution was observed, with the smaller citrate-coated particles solubilizing slightly more than the larger ones (Table 2) (presumably due to larger surface area to volume ratios), similar to prior reports.[37]

For the Ag NPs studied herein, both the size and surface coating were observed to have a significant effect on the magnitude of the antibacterial activity (24 h IC_{50} values based on *E. coli* growth inhibition assay are in Table 2). Within the series of citrate-coated Ag nanomaterials, increasing the size significantly decreased their toxicity toward *Escherichia coli* bacteria (Figure 1a). With a 2-fold increase in Ag nanomaterial particle size, the antibacterial activity of these particles decreased by a factor of 2.5 (Figure 1b). To investigate whether the observed differences in IC_{50} values were due to dissolved Ag ions, as suggested by several previous studies,[2,13−15] we normalized the *E. coli* IC_{50} values for differentially sized Ag-cit particles to the percent of dissolved Ag (as determined by UV−vis spectroscopy) for each type of particle (Figure 1, bottom). Even when normalized for dissolved silver,

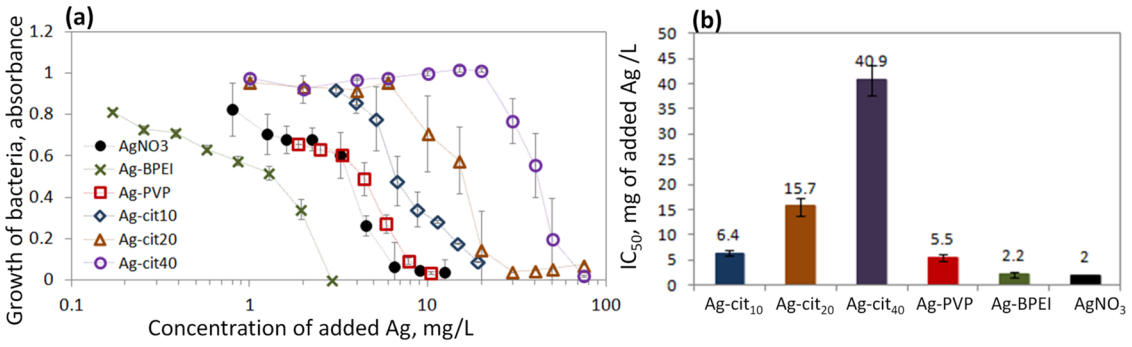

	Ag-cit$_{10}$	Ag-cit$_{20}$	Ag-cit$_{40}$	Ag-PVP	Ag-BPEI	$AgNO_3$
IC_{50}, mg of dissolved Ag/L	0.49	0.89	1.92	0.242	0.59	**2**
IC_{50}, mg of bioavailable Ag/L	1.52	1.2	1.8	2.1	2.4	**2**

Figure 1. Bacterial toxicity of Ag NPs with different size and surface coating. Growth of *Escherichia coli* after 24 h of exposure to Ag NPs or Ag^+ (in the form of $AgNO_3$) as amount of Ag added: (a) 24 h IC_{50} values based on *E. coli* growth inhibition (from (a)) as amount of added Ag or (b) 24 h IC_{50} values normalized to dissolve or bioavailable Ag are shown in the table at the bottom of this figure. The percent dissolution and percent bioavailable Ag^+ for each of the Ag NPs are provided in Table 2.

the IC_{50} values for these particles increased monotonically with size. A reasonable conclusion based on this analysis is that there may be other size-dependent properties in addition to dissolution in bacterial media that makes smaller Ag-cit particles more toxic.

As several previous studies have demonstrated that the fraction of metal that is bioavailable (*i.e.*, has actually entered the cells)—as opposed to the percent dissolution—is the most relevant parameter influencing metal toxicity,[38,39] we also measured the concentration of bioavailable Ag *inside* the bacteria using a genetically engineered biosensor bacterium in which bioluminescence is specifically induced by bioavailable Ag ions.[40] These experiments (see Table 2 and Figure S3 in the Supporting Information) reveal that the increase in % bioavailable silver seen when going from Ag-cit$_{40}$ to Ag-cit$_{10}$ (>7-fold) is significantly greater than the corresponding increase in % dissolution (~1.5-fold). When the IC_{50} values of differentially sized Ag-cit particles were normalized for bioavailable Ag^+, the values all fall roughly within experimental error of each other and are roughly equivalent to that of $AgNO_3$ (Figure 1, bottom). These data support prior studies[38,39] and suggest that the amount of bioavailable/intracellular silver is a better predictor for the toxicity of a particular Ag NP than is the amount of (abiotic) dissolution of the NP. This result is not surprising given that Ag^+ is expected to form complexes with various species (*e.g.*, Cl^-) in biological media, which will effect the amount of Ag^+ that is available to the organism.

Similar to primary size, the surface coating of the Ag NPs had a significant effect on the magnitude of their toxicity. Here, we investigated the properties of Ag-PVP and Ag-BPEI particles which had different surface coatings. It should be noted that, although these particles had similar primary sizes to the Ag-cit$_{20}$ particle (*i.e.*, roughly 20 nm), the observed particle size distributions were quite different both for the primary particles and for the particles dispersed in solution (see Table 1 and Figure S1 in the Supporting Information). The IC_{50} values observed for Ag-BPEI and Ag-PVP were 2.2 and 5.5 mg/L, respectively (Table 1 and Figure 1b). As different coating/stabilizing polymers were used to produce these nanoparticles, we checked whether the coating materials were themselves toxic. No toxicity was observed for citrate, PVP, or BPEI at concentrations that corresponded to the highest concentrations present in nanoparticle stock suspensions (Figure S4 in the Supporting Information). Also, the coating/stabilizing materials had no effect on the toxicity of $AgNO_3$. The most toxic nanoparticle, Ag-BPEI, had an IC_{50} value almost similar to that of $AgNO_3$ (Figure 1b), consistent with an earlier report in a different bacterial species.[11] Because the percent dissolution of Ag-BPEI in bacterial media is significantly lower than that of $AgNO_3$ (Table 2), it is not possible to explain the magnitude of toxicity of Ag-BPEI NP with the amount of dissolved silver.

By analyzing bioavailable Ag inside bacterial cells using bacterial bioreporters, we showed that the relative concentrations of bioavailable silver for Ag-PVP and Ag-BPEI are substantially more than one would predict based on the concentration of dissolved silver in these samples. As a result, when the IC_{50} values of Ag-PVP and Ag-BPEI were normalized for the concentration of bioavailable Ag^+ (Figure 1, bottom), the IC_{50} values for the entire series of Ag NPs were roughly on par with that of $AgNO_3$ (~2 ± 1 mg/L). Again, these data suggest that the concentration of bioavailable/intracellular silver generated by a particular Ag NP is a better predictor for the toxicity of that NP than is the amount of (abiotic) dissolution of the NP. Also, it is clear that both the size and the surface properties of Ag NPs play an important role in *delivery* of Ag to bacterial cells

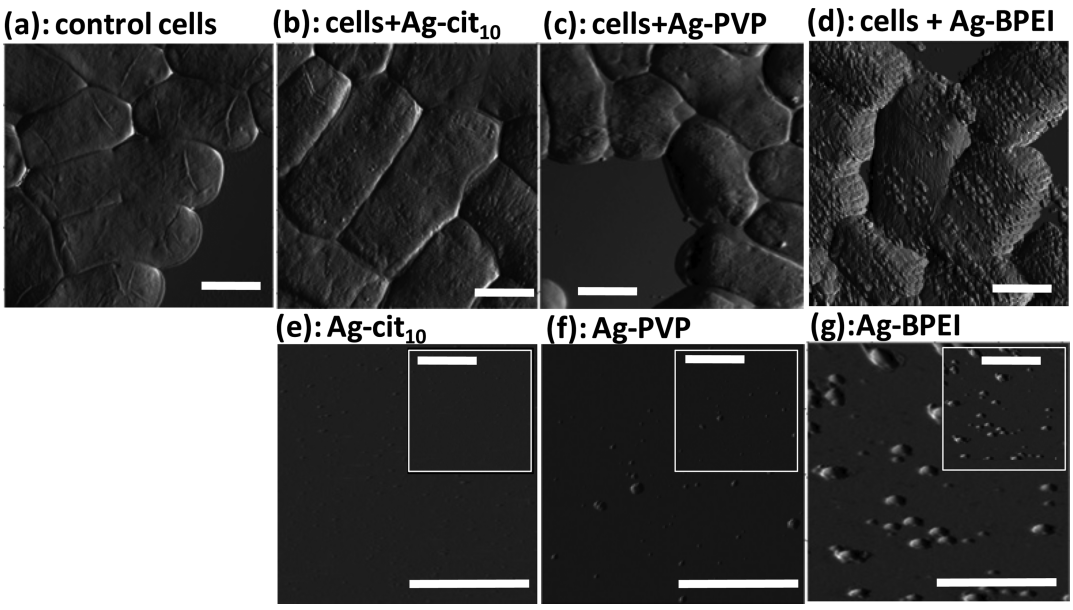

Figure 2. Attachment of Ag nanomaterials onto the surface of *E. coli* cells. (a) Bacterial cells with no NPs treatment. (b–d) Atomic force images of bacterial cells incubated with different Ag NPs (IC_{10} concentrations were used). (e–g) Abiotic suspensions of NPs. Scale bar represents 1 μm. Insets in (e–g) show the images at lower magnification.

via mechanisms that involve more than simply dissolution of Ag^+ in bacterial media. These data also highlight an additional question, which is *why* is it that Ag-PVP and Ag-BPEI deliver more Ag^+ to the inside of the bacterial cells compared to what one would expect based solely on the amount of dissolved Ag that these particles produce in bacterial media. Prior reports have suggested that surface charge can play an important role in how effectively NPs interact with the negatively charged bacterial surface.[41−43] Indeed, the IC_{50} values for Ag-cit_{20}, Ag-PVP, and Ag-BPEI correlate linearly (r = 0.89) with their ζ-potentials (Table 1 and Figure S5 in the Supporting Information), even though the primary size distributions for these particles are not identical. In addition, when 1 mg/L of Ag-BPEI NPs was added to *E. coli* cells (which exhibit a negative ζ-potential), the ζ-potential of the resulting mixture turned positive (Figure S6 in the Supporting Information). In addition, using atomic force microscopy (AFM), we were able to observe Ag-BPEI NPs adhered to the bacterial surface, while almost no such attachment was observed for negatively charged particles (Figure 2). Likewise, TEM visualization of Ag-BPEI-exposed cells showed that some of the positively charged Ag-BPEI NPs had fused with the bacterial cell wall (Figure S7 in the Supporting Information). Despite earlier reports of intracellularization of Ag nanoparticles,[44] no internalized Ag nanoparticles were observed under the conditions in which these TEM experiments were performed (Figure S7 in the Supporting Information). Likewise, AFM and TEM images indicated also that a small number of the Ag-PVP NPs (*versus* no Ag-citrate particles) are attached to the bacterial surface. These observations are consistent with a mechanism in which the positive charge of the Ag-BPEI particles (and to a lesser extent the moderately negatively charged Ag-PVP particles) allows these particles to bind to bacterial surfaces and hence serve as a more effective delivery agent for Ag, hence increasing the magnitude of their toxicity. What these results, and similar results from other *prior* studies, do *not* do, however, is provide detailed insights into the pathways involved in how bacteria respond to the toxic Ag nanoparticles.

High-Throughput Screening of a Library of Single Gene Deletion Strains for *E. coli* Provides Detailed Insights into How This Organism Responds to Different Ag Nanoparticles. To address the question of which pathways are involved in the bacterial response to different Ag NPs, and whether these pathways are the same as that for ionic Ag, we conducted a series of high-throughput experiments in which the impacts of Ag-BPEI, Ag-PVP, Ag-cit_{20}, Ag-cit_{10}, or $AgNO_3$ NPs on 4159 different *E. coli* single gene deletion strains (GDS)[24] were examined. In these experiments, the gene deletion mutants are arrayed in microwell plates and then screened to determine whether they are more sensitive to each of the different Ag formulations than the parent strain is. A similar approach has been used by a number of groups to study the ways in which *E. coli* and the eukaryote *S. cerevisiae* respond to different classes of antibiotics or types of environmental stress.[15,26−30,42] Of these reports, a recent paper by Nichols *et al.*[30] is particularly notable because the authors reported growth profiles for the library of *E. coli* GDS under >300 conditions. When analyzed using a gene network based clustering strategy, drugs that were known to have the same cellular target(s) tended to cluster together and that this type of analysis can provide

clues to the modes of action of drugs where the molecular target is unknown.[30] We recently reported that a similar approach can be applied to elucidate which pathways are important to how *E. coli* responds to toxic nanoparticles and to infer the mechanisms of toxicity of these particles by comparing the results to small molecule analogues with known mechanisms.[23] In the experiments performed herein, the library of *E. coli* GDS was screened on 384-well plates in the presence of $AgNO_3$ or Ag-BPEI, Ag-PVP, Ag-cit$_{20}$, and Ag-cit$_{10}$ NPs, at a concentration of Ag corresponding to the IC_{10} for that material for the parent strain. Each experiment was performed in quadruplicate so that the reproducibility of the results could be assessed. A detailed explanation of the method used for analyzing these data is provided in the Supporting Information, as well as an example of the results of the statistical methodology used to assess the reproducibility of the results for specific Ag NPs (Figure S8). Highly reproducible results were obtained for replicates within each Ag species studied. Ag-cit$_{40}$ was not studied using the HTS of GDS approach because the IC_{10} for this material is sufficiently high that the amount of material that would be required for the HTS experiment would be prohibitively expensive. At the IC_{10} concentration for each material, the parent strain shows relatively little growth impairment, and more sensitive strains can be readily identified based on whether they show significant growth impairment compared to the parent strain. Those strains which showed sensitivity toward *any* of the Ag formulations in the initial screen (2417 "initial hits") were consolidated into a smaller number of 384-well plates, and complete growth curves were obtained for each strain for each Ag formulation. The IC_{50} values for 995 strains that were confirmed sensitive for $AgNO_3$, Ag-BPEI, Ag-PVP, Ag-cit$_{20}$, or Ag-cit$_{10}$ NPs are provided in Table S2 in the Supporting Information, along with the gene name, gene ID, and function (if known). Corresponding data for a cationic nanoparticle that does not contain Ag (PS-NH_2) that we have reported previously[23] are also provided in Table S2 in the Supporting Information for comparison. As can be seen from a cursory inspection of Table S2, the results for each of the different toxicants studied were unique. This variability that was observed for the responses of *E. coli between* different types of nanoparticles/silver species is in stark contrast to the high level of reproducibility observed between different replicates for a given nanoparticle/silver species (Figure S8). Two different types of complementary analyses were performed on these data and to determine what similarities, if any, exist between the responses seen for the different silver species: one in which no information about the biological function of the genes missing from the sensitive gene deletion strains was used in the initial clustering ("self-organizing map" analysis)[45] and one in which prior knowledge about interactions between genes and gene products corresponding to the sensitive gene deletion strains was used for the initial clustering ("DAVID" analysis).[46] Here, the results of each of these analyses are discussed in turn.

Self-Organizing Maps of High-Throughput Gene Deletion Strain Data Reveal "Ag-Specific" Response Genes and Overall Picture of How E. coli Responds to Different Ag NPs Varies from Particle to Particle. A primary advantage of self-organizing map (SOM) analyses is that they provide a methodology for visualizing complex multidimensional data sets in a way that similarities are readily visually apparent.[45] This method also allows quantitative information (such as the IC_{50} data for each of the strains) to be explicitly integrated into the analysis, so that statistically significant correlations between different subsets of data can be determined. In Figure 3, the larger SOM on the left provides a two-dimensional projection of the multidimensional high-throughput screening gene deletion strain (HTS GDS) data, where gene deletion strains that behave similarly are clustered with each other. The SOM consists of an array of hexagons ("SOM units"), where each unit represents a set of gene deletion strains (GDS) of similar response to stimuli, and the proximity of the units in the SOM is indicative of their similarity. The color of the unit represents the average magnitude of the response of the GDS in that unit, with dark red representing the most sensitive strains (~50% decrease in growth compared to parent strain) and dark blue representing strains that in the presence of the stimulus grow the same as the parent strain. The large map on the left of Figure 3 depicts clusters of SOM units (and hence the gene deletion strains within these clusters) that behave in roughly the same way in response to all of the toxicants (*i.e.*, to $AgNO_3$, Ag-cit$_{10}$, Ag-cit$_{20}$, Ag-PVP, and Ag-BPEI), with the color of each of the 19 clusters representing the average response of the GDS within that cluster. Component planes of the SOM that correspond to the HTS GDS data for each individual Ag formulation are shown on the right-hand side of Figure 3.

Several important observations and inferences can be made on the basis of these maps. First, the orange cluster on the main SOM map (large map on the left of Figure 3) depicts those gene deletion strains that respond, on average, most significantly to all the silver formulations. This cluster can reasonably be interepreted as a fingerprint of an average "silver-specific" response. There were 35 common mutants that were sensitive to all the tested Ag nanoparticles and also $AgNO_3$. (These genes are listed in the orange box in the middle of Figure 3; a list of the gene deletion strains in each of the units and clusters in the entire SOM is provided in Table S3 in the Supporting Information. The locations of specific SOM units and clusters are depicted in Figure S9 in the Supporting Information.) The genes corresponding to these mutants include *cueR*, which is a Cu(I)-dependent transcriptional regulator, and *cusS*, which is a part of two-component regulatory system

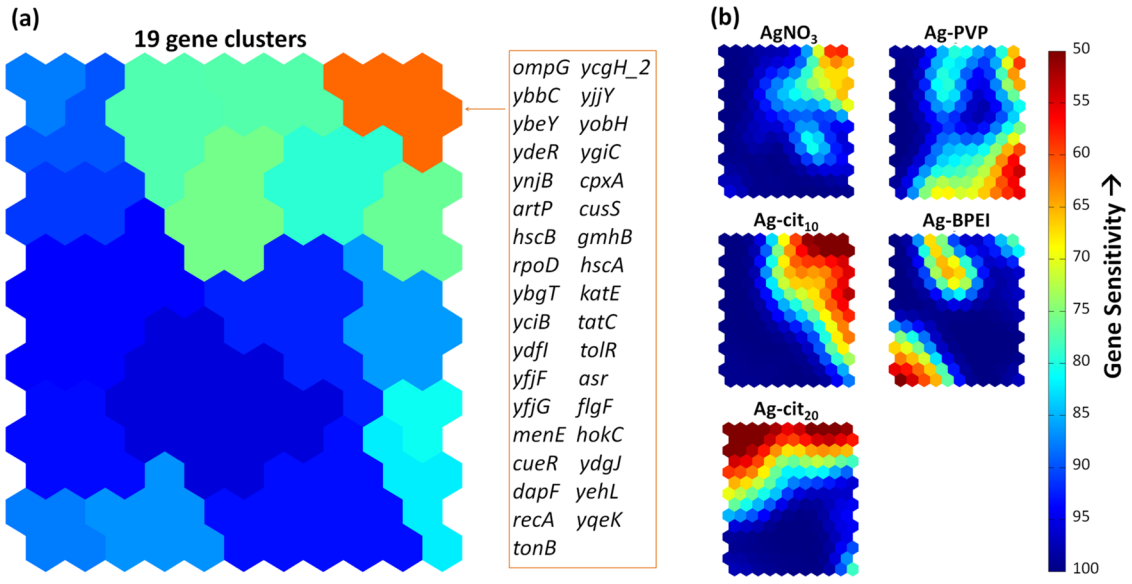

Figure 3. Self-organizing map analysis of *E. coli* gene deletion strains that are more sensitive than the nonmutated *E. coli* strain to $AgNO_3$, Ag-cit_{10}, Ag-cit_{20}, Ag-PVP, and/or Ag-BPEI. The SOM is a two-dimensional projection of the multidimensional high-throughput screening gene deletion strain data, organized to show which groups of gene deletion strains behave similarly.[43] Each hexagon ("SOM unit") represents a set of gene deletion strains that respond similarly to stimuli. The color of the unit represents the average magnitude of the response of the GDS in that unit, with dark red representing the most sensitive strains (~50% decrease in growth compared to parent strain) and dark blue representing strains that grow the same as the parent strain in the presence of toxicant. The large map (a) depicts clusters of SOM units (and hence the gene deletion strains within these clusters) that behave roughly similarly in response to all of the toxicants (*i.e.*, to $AgNO_3$, Ag-cit_{10}, Ag-cit_{20}, Ag-PVP, *and* Ag-BPEI) with the color of each of the 19 clusters representing the average response of the GDS within that cluster. The GDS in the orange cluster (genes listed in the orange box next to the large SOM) can be interepreted as a fingerprint of an average "silver-specific" response. Component planes of the SOM that correspond to the HTS GDS data for each individual Ag formulation are shown in (b). The observation that there is no significant similarity between the individual component planes suggests that the patterns of responses for the different Ag formulations are distinct. Ag-cit_{10} is the only Ag NP that shows a moderate correlation with $AgNO_3$ (Pearson's correlation coefficient = 0.58). Pearson's correlation coefficient values for all of the pairs of Ag formulations are provided in Table S2 in the Supporting Information.

responsible for the expression of CueR. CueR in turn activates a cascade of Cu resistance systems in *E. coli*.[47] Ag and Cu ions are known to be transported and detoxified *via* similar pathways in *E. coli*.[48] Therefore, the observation that $AgNO_3$ and Ag nanoparticles affect the bacterial copper resistance system indicates that all of the Ag formulations studied herein affect bacterial cells at least in part *via* dissolved Ag ions. It is worth mentioning that *cueR* single gene mutant has been also demonstrated to be sensitive toward a different Ag nanomaterial.[44] *KatE* and *recA* are also among these genes whose absence results in a Ag-sensitive bacterial phenotype. *KatE* encodes a catalase that is induced in the conditions of high levels of peroxide, and *recA* is induced by DNA damage. Indeed, earlier studies have shown that both $AgNO_3$ and Ag NPs induce oxidative stress in bacterial cells,[13,18,41] which may also lead to the DNA damage. In addition, several inner membrane-related proteins (*dcuC*, *sdhD*, *tatC*, *tolR*, *tonB*, *trkA*) were found among the genes whose absence resulted in sensitive phenotype for all the tested Ag formulations. Approximately one-third of the genes whose absence resulted in sensitive phenotype toward $AgNO_3$ or Ag NPs were of unknown or hypothetical function. Of the 35 genes which, when deleted, led to a Ag nanomaterial or $AgNO_3$-sensitive phenotype, only 6 (*cpxA*, *tatC*, *tolR*, *ybgT*, *yfjF*, and *yqiC*; ~17%) belong to a group of multi-stress-responsive genes[30] and only 8 (*flgF*, *hscB*, *gmhB*, *recA*, *ybbC*, *yciB*, *yfjF*, and *yfjG*; ~23%) are also responsive to toxic 60 nm polystyrene nanoparticles (PS-NH_2) (see Table S2 in the Supporting Information). Second, the SOM patterns of responses for the different Ag formulations are each distinct, indicating that there is no significant similarity between the individual component planes. Ag-cit_{10} is the only Ag NP that shows a moderate correlation with $AgNO_3$ (correlation coefficient = 0.58). The correlation coefficient values for all of the pairs of Ag formulations are provided in Table S4 in the Supporting Information. Because we hypothesized that the specific toxicological properties of positively charged Ag-BPEI particles were due to their highly positive ζ-potential, we also performed a clustering analysis in which we included corresponding data from our earlier study[41] for 60 nm polystyrene (PS-NH_2) particles that exhibited similar high positive ζ-potential (see Figure S10 in the Supporting Information. The HTS GDS data for the PS-NH_2 NP are also provided in Table S2. The correlation coefficient between Ag-BPEI and PS-NH_2 particles was 0.36, indicating that the data are weakly correlated, suggesting that there may be some component of the response that is specific to cationic nanomaterials (see below).

Functional Classification (DAVID) Clustering Analysis Provides Detailed Insights into the Different Gene

TABLE 3. Grouping of Gene Deletion Strains Sensitive to Each Ag Formulation to Functional Clusters Using DAVID Software[a]

			clustering of genes according to DAVID[c]		
	number of sensitive mutants	number of sensitive mutants that are multi-stress-responsive mutants[b]	cluster (number of genes in cluster)[d]	main molecular function annotation term associated with the cluster (number of genes in this GO term)	*p* value[e]
$AgNO_3$	222	18	cluster 1.1 (56)	ATP binding (12)	3.7×10^{-5}
			cluster 1.2 (6)	metal binding (6)	1.5×10^{-7}
			cluster 1.3 (4)	antioxidant activity (3)	4.6×10^{-5}
			cluster 1.4 (4)	protein transporter activity (2)	1.9×10^{-2}
			cluster 1.5 (4)	flagellar motor activity (4)	8.4×10^{-6}
			cluster 1.6 (10)	transition metal ion binding (3)	2.8×10^{-1}
Ag-cit_{10}	312	19	cluster 2.1 (88)	ATP binding (17)	7.5×10^{-6}
			cluster 2.2 (4)	4Fe-4S cluster binding (4)	2.2×10^{-5}
			cluster 2.3 (4)	protein transporter activity (2)	1.9×10^{-2}
			cluster 2.4 (4)	antioxidant activity (3)	4.6×10^{-5}
			cluster 2.5 (9)	cell surface antigen activity (lipopolysaccharides) (6)	8.3×10^{-15}
			cluster 2.6 (6)	motor activity (4)	8.7×10^{-3}
Ag-cit_{20}	471	24	cluster 3.1 (103)	quinone binding (15)	1.3×10^{-4}
			cluster 3.2 (15)	protein kinase activity (7)	2.6×10^{-8}
			cluster 3.3 (7)	flagellar motor activity (4)	1.9×10^{-7}
			cluster 3.4 (4)	metal ion binding (4)	3.9×10^{-3}
			cluster 3.5 (13)	cell surface antigen activity (lipopolysaccharides) (8)	6.6×10^{-16}
			cluster 3.6 (9)	metal cluster binding (9)	1.2×10^{-11}
			cluster 3.7 (5)	antioxidant activity (4)	2.1×10^{-5}
Ag-PVP	515	15	cluster 4.1 (100)	ATPase activity (24)	2.4×10^{-12}
			cluster 4.2 (24)	ATP binding (16)	7.1×10^{-10}
			cluster 4.3 (7)	metal ion binding (3)	2.4×10^{-1}
			cluster 4.4 (19)	iron ion binding (19)	6.4×10^{-22}
			cluster 4.5 (9)	flagellar motor activity (4)	1.9×10^{-7}
			cluster 4.6 (5)	antioxidant activity (3)	3.1×10^{-4}
			cluster 4.7 (8)	cell surface antigen activity (lipopolysaccharides) (3)	7.6×10^{-5}
Ag-BPEI	241	18	cluster 5.1 (61)	oxidoreductase activity, acting on NADH or NADPH (4)	5.6×10^{-3}
			cluster 5.2 (7)	quinone binding, ubiquinone biosynthesis (7)	1.3×10^{-13}
			cluster 5.3 (12)	cell surface antigen activity (lipopolysaccharides) (9)	8.0×10^{-19}
			cluster 5.4 (5)	antioxidant activity (4)	1.1×10^{-3}
PS-NH_2[f]	99[f]		cluster 6.1 (10)	cell surface antigen activity (lipopolysaccharides) (7)	4.7×10^{-4}
			cluster 6.2 (6)	quinone binding, ubiquinone biosynthesis (6)	1.5×10^{-11}
			cluster 6.3 (18)	iron ion binding (4)	2.0×10^{-2}

[a] The number and functional classification of genes that were absent in bacterial mutant strains which were confirmed to be sensitive towards Ag^+ ($AgNO_3$) and/or different Ag NPs studied herein. Cationic amino-functionalized (PS-NH_2) nanoparticles are included for comparison. [b] Eighty-nine multi-stress-responsive mutants were identified in ref 29. [c] DAVID, Database for Annotation, Visualization and Integrated Discovery v6.7, http://david.abcc.ncifcrf.gov/. [d] For clustering, high classification stringency (similarity threshold 0.5, multiple linkage threshold 0.5, group membership 5) was used. [e] Fisher exact *p* value for gene enrichment analysis (calculated automatically in the DAVID database). [f] Only mutants that are both sensitive to PS-NH_2 NPs and to either Ag^+ or one of the Ag NPs are reported here. A complete list of mutants that are sensitive to amino-functionalized polystyrene nanomaterials are reported in ref 23.

Clusters Involved in How E. coli Responds to Different Ag NPs and How These Compare to Ionic Ag. In addition to the SOM analysis described above, the HTS GDS data were also analyzed using an online Database for Annotation, Visualization, and Integrated Discovery (DAVID; http://www.david.niaid.nih.gov).[46] DAVID can be used to facilitate interpretation of genome-scale data sets such as the ones generated in this study by integrating prior data from a variety of sources about the relationships between different genes and proteins (*e.g.*, gene ontologies, protein domain, and biochemical pathway membership) to provide insights into the analyses that are performed. Here, the DAVID functional classification tool was used to cluster gene deletion strains that were confirmed to be sensitive to each of the specific Ag formulations and to identify the most significant gene ontology (GO) molecular function annotations for each gene cluster. The resulting lists of annotated gene clusters for each Ag formulation are provided in Table 3, and the individual genes found within each of the clusters are listed in Table S5 in the Supporting Information. The results of the DAVID analysis provide a clear picture of which pathways are involved in how *E. coli* responds to silver stress in general (*i.e.*, pathways that are common to all of the Ag NPs and $AgNO_3$) as well as which pathways appear to be "nano-specific" responses (*i.e.*, are represented in the data for the Ag NPs, but not ionic Ag^+), as well as which pathways appear to be specific to particular nanomaterials or classes of nanomaterials. A primary

example of a gene cluster that was associated with each of the different silver formulations is *antioxidant activity* (Table 3), for which 3−4 gene deletion strains showed up as sensitive for each of the Ag formulations (see specific gene deletion strains in Table S5 in Supporting Information). As this cluster did not turn up for toxic 60 nm polystyrene nanoparticles (PS-NH_2), this pathway may be considered silver-specific.[13,18,41] Another pathway that appeared to be silver-specific was bacterial flagellar motor activity (Table 3). Specifically, a series of *flg* mutants were sensitive to $AgNO_3$ and Ag NPs. Although this cluster was not clearly distinguished in the case of Ag-BPEI NPs, *flgD*, *flgGm*, *flgJ*, and *flgM* were also among confirmed sensitive mutants for this particle (Table S2 in Supporting Information). Interestingly, Ag has indeed shown to have an effect on bacterial outer membrane and flagellar formation also in earlier studies.[49] The primary example we observed of a pathway that appears to be a nano-specific response is that clusters of gene deletion strains where the deleted genes encode for *cell-surface antigen activity (lipopolysaccharides)* showed up for all of the nanoparticle formulations studied herein (including PS-NH_2), but not for $AgNO_3$ (ionic Ag) (Table 3). The genes in this cluster are mostly *rfa* genes that are responsible for the assembly of the outer membrane lipopolysaccharides (LPS).[50] According to Nichols *et al.*,[30] *rfa* genes belong to the group of multi-stress-responsive genes. LPS are known to provide a negative surface charge and additional protection for bacterial cells against cationic small molecule toxins.[51,52] The suggestion that the LPS layer may function as a protective layer against small cationic molecules, cationic nanoparticles,[23] and nanoparticles more generally deserves a closer study. In addition to the silver-specific and nano-specific responses, there are a number of "particle-type-specific" responses observed or responses that appeared for only a subset of the particles studied. Consistent with the results of the SOM analysis that showed similar clustering patterns for cationic Ag-BPEI and polystyrene PS-NH_2 particles, we found that there was a cluster (quinone binding, ubiquinone biosynthesis, which includes the *ubiE*, *ubiF*, *ubiH* mutants) that was common to these positively charged NPs (Table 3). In our previous study, we demonstrated that the sensitivity of these mutants to the cationic PS-NH_2 particle correlated with their sensitivities to a cationic small molecule, polymyxin B, and that these genes appeared to be important in how the organism mitigates stress caused by reactive oxygen species formed at the cell surface due to the defects in the electron transport chain.[23] The current data suggest that exposure to cationic Ag NPs may also result in production of cell-membrane-associated ROS and that the organism's ability to react to this insult may be important to its ability to mitigate the harmful effect of cationic Ag NPs.[30]

Taken together, the results of the SOM and DAVID analyses clearly indicate that while dissolution of Ag and the resulting toxicity of Ag^+ play a role in the toxicity of the Ag NPs, different pathways are also important (and in some cases, more important) in how *E. coli* responds to specific Ag nanoparticles. In particular, cationic Ag-BPEI elicited a response more similar to a cationic nanoparticle that contains no silver (PS-NH_2) than to the responses for either ionic Ag or any of the other Ag NPs tested, and only one of the Ag NPs studied (Ag-cit_{10}) elicited an overall response that was quantitatively similar to that of ionic Ag. Some gene clusters (*e.g.*, cell-surface antigen activity (lipopolysaccharides)) identified appeared to correlate with a nano-specific response (*i.e.*, appeared as significant for all of the NPs studied, but not ionic silver), whereas others appeared to be important for only a subset of the particles studied.

CONCLUSIONS

The study reported herein supports prior studies that show that magnitude of toxicity of negatively charged Ag nanomaterials correlates with the amount of dissolved Ag ion that these particles produce in solution and demonstrates that the ability of positively charged Ag NPs to tightly interact with bacterial surface results in high concentrations of bioavailable Ag ions from these particles. Positively charged particles also interfere with the normal function of the bacterial electron transport chain and are responsible for ROS formation at the cell membrane. Studies using gene deletion strains also revealed that, although there are some common pathways involved in how bacteria respond to silver stress, there are other pathways that appear to correlate with nanoparticle-related stress. Reactive oxygen production and impairment of flagellar activity were observed for a broad range of silver species. By contrast, effects on cell outer surface lipopolysaccharides appear to be nanoparticle-specific. These data suggest that, although Ag NPs toxicity is on a large scale mediated by dissolved Ag ions, the way in which the particles interact with bacterial cells and some of the pathways involved in the toxicity of the particles are highly dependent on nanoparticle physicochemical properties. These results have important implications for understanding the mechanisms of toxicity of silver nanomaterials and for how silver nanoparticles are regulated and tested going forward.

MATERIALS AND METHODS

Chemicals and Nanoparticles. *Media Components.* Bacterial growth media (Luria−Bertani, LB, Lennox) was from EMD Chemicals (Merck, Darmstadt, Germany); the pH of the final media was 7. Fetal bovine serum (FBS) was purchased from Gemini-BioProducts (CA, USA); kanamycin sulfate was purchased from Sigma-Aldrich; phosphate buffered saline (PBS, pH 7.4) was from GIBCO (Invitrogen, CA, USA), and humic acid was purchased from Sigma-Aldrich.

Nanoparticles. Citrate-stabilized Ag NPs (Ag-cit) with advertized sizes of 10, 20, and 40 nm were purchased from Nanocomposix (CA, USA). The nanomaterials were supplied as 1 mg/mL aqueous dispersion stored in 0.5 g/L of sodium citrate solution. Polyvinylpyrrolidone (PVP)-stabilized and branched polyethyleneimine (BPEI)-stabilized Ag NPs (Ag-PVP and Ag-BPEI) were synthesized in our laboratory. For the synthesis of Ag-PVP, solutions of 9.4×10^{-3} M $AgNO_3$ (50 mL), 15.8×10^{-3} M $NaBH_4$ (150 mL), and 0.75% PVP (PVP 40, M_w = 40 000, Sigma-Aldrich) (50 mL) were prepared. The three solutions were delivered with volume ratios of 1 $AgNO_3$/1 PVP/3 $NaBH_4$ to an empty beaker using a multichannel peristaltic pump (Ismatic, IPC, 22 channels). The beaker was stirred vigorously using a stir bar on a stir plate. After the total volume of the three solutions was delivered to the beaker, the pH of the resulting nanoparticle suspension was adjusted to 4.0 using a 5% HNO_3 solution.

For the synthesis of BPEI-Ag, 0.085 g of *N*-(2-hydroxyethyl)-piperazine-*N*′-2-ethanesulfonic acid (HEPES) was dissolved in a 100 mL solution of 9.4×10^{-3} M $AgNO_3$ (prepared in Milli-Q water). The pH of the mixture ($AgNO_3$/HEPES) was adjusted to a pH of 6.5 using 1% branched polyethyleneimine solution (BPEI, M_w = 1.20 kg mol^{-1}, Polysciences Inc.). The mixture was exposed for 80 min to UV irradiation using a standard low-pressure mercury arc lamp.

The synthesized Ag-PVP and Ag-BPEI NPs were purified from the residual chemicals, especially ionic silver by an ultrafiltration system (Spectrum Laboratories, Inc., USA) equipped with a 10 kDa polyethersulfone (PES) membrane (MidiKros Hollow Fiber Module (P-X3-010E-300-02N). The concentration of silver in suspensions of all the nanomaterials was determined by graphite furnace atomic absorption spectrometry (GF-AAS, AAnalyst 700, Perkin-Elmer). Lumina hollow cathode lamp of single element (Ag) was used in the measurement. Five microliters of matrix modifier (3 g/L Pd + 2 g/L $Mg(NO_3)_2$) was added to each sample of 20 μL using an autosampler for improved analytical quality.

Transmission electron microscopy (TEM, JEOL 1200 EX, accelerating voltage 80 kV) was used to determine the morphology and primary size of the nanomaterials. Samples were prepared by placing a drop of an aqueous suspension of the nanomaterial on a carbon-coated TEM grid and waiting until the water evaporated. For each type of particle, diameters of 25 particles were measured from TEM images to determine the average primary sizes and their standard deviations.

Preparation of Nanoparticle Dispersions in Liquid Media and Characterization. All the Ag NPs were prepared and stored in liquid state. Further dilutions were performed in DI water in bacterial growth media (LB) supplemented with 5% FBS. For dispersion in bacterial growth media, first 10% of FBS was added to the NP stock dispersion and the mixture was sonicated in a water bath (Branson 2510, CT, USA) for 15 min. Then, 2-fold concentrated LB media (EMD Chemicals) supplemented with 50 μg/mL at a ratio of 1:1 was added, and the mixture was again sonicated for 15 min in a water bath.

Hydrodynamic diameter (D_h) of NPs dispersed in DI water or in bacterial growth media was measured using a high-throughput DLS instrument (Wyatt Technology Corporation, CA, USA). Blank water or growth medium was always used as control and, if needed, was taken into account in calculation of the final D_h values. The ζ-potential values of NPs suspended in aqueous solution were determined using a ZetaPALS ζ-potential analyzer (Brookhaven Instruments Ltd., UK). The surface charge (ζ-potential) of Ag NPs was not measured in bacterial growth media due to the interference of salts and organic components that are present in the nutrient-rich LB media with the electrophoretic mobility measurement.

Determination of Dissolved Silver. The amount of dissolved Ag was determined using UV−vis spectrometry. UV−vis spectrometry of nanoparticles was performed by scanning the absorption of Ag NP suspension from 300 to 800 nm using SpactraMax5 plate reader; a measurement was recorded every 2 nm. For the measurement, 100 μL of the 12.5 mg/L suspension of Ag nanoparticles either in DI water or in LB media was pipetted onto a clear 96-well polystyrene microplate in triplicate, and the absorption was measured immediately (0 h) or after 24 h of incubation at 37 °C. During prolonged incubation, the plate was covered with a lid and the plate was shaken before the measurement to avoid settling of particles.

For calculation, the absorption values of blank DI water or LB media were subtracted from those of Ag NP suspensions in water or LB media, respectively. Resulting absorption values were plotted against the wavelengths at 0 h (beginning of the test) and after 24 h of incubation (for the duration of bacterial toxicity test, see below) at 37 °C. The difference in area under the UV−vis curves (from 300 to 800 nm) between 0 and 24 h was used to quantify the decrease in Ag NP concentration. This method was adapted from ref 32. The amount of dissolved silver was also quantified by atomic absorption spectroscopy (preceded by centrifugation to remove nanoparticles in solution). The additional details on the method used to determine the concentration of dissolved silver using atomic absorption spectroscopy is included in the Supporting Information.

Assessment of Bioavailable Silver. Bioavailable Ag was assessed by using genetically engineered biosensor bacteria in which bioluminescence is specifically induced by bioavailable Ag ions.[40] For this assay, the Ag NPs were dispersed as described above. Biosensor bacteria *E. coli* MC1061(pcueR/pcopAlux) and constitutively bioluminescent control strain *E. coli* MC106-(pSLlux)[40] were pregrown overnight in LB media supplemented with 100 μg/mL of ampicillin and 10 μg/mL of tetracycline or 100 μg/mL of ampicillin, respectively. The overnight culture was diluted to an OD of 0.05 and subsequently grown to an OD of 0.6. Prior to the test, this culture was 6-fold diluted with 5% FBS supplemented LB media prior the test. Ag NPs were also diluted in 5% FBS supplemented LB media, and 25 μL of each concentration (each concentration was analyzed in triplicate) was pipetted onto the wells of a 384-well plate; blank medium with no NPs was used as a control. Twenty-five microliters of diluted bacterial culture was added onto the wells, and the plates were incubated for 2 h at 30 °C. After that, bacterial bioluminescence in RLU was measured and induction of Ag biosensors by bioavailable Ag was calculated by the following formula:

$$\text{induction} = \frac{RLU_{S,S}}{RLU_{S,B}} \times \frac{RLU_{C,B}}{RLU_{C,S}}$$

where $RLU_{S,S}$ is bioluminescence of the Ag sensors in Ag-containing sample ($AgNO_3$ or Ag NP), $RLU_{S,B}$ is the bioluminescence of these bacteria in blank media, $RLU_{C,B}$ is the bioluminescence of constitutively bioluminescent strain in blank media, and $RLU_{C,S}$ is the bioluminescence in the Ag sample ($AgNO_3$ or Ag NP). The amount of bioavailable Ag in each of the Ag NP samples was calculated by comparing the concentrations of $AgNO_3$ and Ag NPs at which 2-fold induction of the Ag biosensors was achieved (LOD_{AgNP} and LOD_{AgNO_3}, respectively); bioavailable concentration of Ag was calculated using the equation

$$\text{bioavailable Ag} \quad (\%) = \frac{LOD_{AgNO_3}}{LOD_{AgNP}} \times 100$$

Assessment of Antimicrobial Activity of Ag Nanoparticles. *Growth Assay Using E. coli Nonmutated Strain BW25113 and Determination of IC_{50} Values for Ag NPs.* Twenty milliliters of bacterial growth media was inoculated with one colony of *Escherichia coli* strain BW25113(pACYC117)[23] from an LB agar plate and bacteria were grown overnight. Fifty microliters of the overnight culture was pipetted onto a 384-well plate; this plate was used later to inoculate the test plate. For the test plate, 50 μL of the diluted Ag NP dispersion in bacterial growth media (LB supplemented with 5% FBS and 25 μg/mL of kanamycin) was pipetted onto another clear 384-well polystyrene microplate. Usually, a dilution factor of 1.5 was used to prepare the Ag NP dilutions, and each dilution was analyzed in nine parallels. Nine parallels of growth media without any Ag compounds were also added to each plate. The test plate with Ag NPs and media controls was inoculated with the overnight bacterial culture by using a plastic 384 pin replicator (Genetix Molecular Devices). When plates were replicated, the replicator was inserted to the bacterial plate; each pin of the replicator was expected to pick up about 1−2 μL of bacteria. Next, the replicator was inserted into the wells of the test plate. Abiotic controls (no bacteria inoculated)

were included for blank media and each Ag NP control. The microplates were incubated at 37 °C, and absorbance at 600 was registered during 24 h using Biotek Synergy plate reader. Bacterial growth after 24 h of incubation was calculated using the following formula:

$$\text{growth} \quad (\%) = \frac{(A_{NM,B} - A_{NM,A})}{(A_{BL,B} - A_{BL,A})} \times 100$$

In this equation, $A_{NM,B}$ is absorbance of bacterial culture with nanomaterials (average of 9 replicates), $A_{NM,A}$ is absorbance of an abiotic sample of the same concentration of nanomaterials (average of 3 replicates), $A_{BL,B}$ is absorbance of bacterial culture in blank media (average of 9 replicates), and $A_{BL,A}$ is absorbance of an abiotic sample of the blank media (average of 3 replicates). Each Ag NP was tested three times. IC_{50} values with 95% confidence intervals for each nanomaterial were calculated using a nonlinear fit of a log-normal distribution in GraphPad Prism program.

Growth Assay with Genome-Wide Collection of E. coli Single Gene Deletion Mutants and Determination of IC_{50} Values for Mutant Strains. The detailed description of methodology used for the toxicity analysis with an array of 4159 *E. coli* single nonessential gene mutant strains is given in ref 23. Briefly, first the growth of the mutant collection in parallel to the nonmutated *E. coli* wild-type strain was tested in the presence of one concentration of Ag NPs that was equal to $\sim IC_{10}$ values for the wild-type *E. coli* strain (*i.e.*, 1.8 mg/L of Ag-cit$_{10}$, 8 mg/L of Ag-cit$_{20}$, 3.8 mg/L of Ag-PVP, 1.4 mg/L of Ag-BPEI, 0.7 mg/L of $AgNO_3$). The growth assay was performed in 384-well microplates with appropriate controls (bacterial growth with NPs and abiotic controls using both nanomaterials and growth media as well as wells containing the nonmutated *E. coli* wild-type strain) on each plate. Each plate was incubated at 37 °C for 24 h and the optical density (OD) of the cultures was measured using a SpectraMax M5 plate reader (Molecular Devices, CA, USA). Before measurement, the plates were shaken to ensure a uniform distribution of both bacterial cells and test compound in the wells.

Each experiment was performed in at least quadruplicate to ensure that only those strains which reproducibly showed a statistically significant increase in sensitivity to a particular toxin were considered as "hits". The data were analyzed as described in ref 23. (See also additional details for the materials and methods provided in Supporting Information.) Briefly, the growth (as measured by the optical density at 24 h) of each mutant strain with or without a specific toxicant added was compared to that of the nonmutated *E. coli* wild-type strain. Criteria for selecting more sensitive *E. coli* single gene deletion mutants were false discovery rates less than 1% (q value ≤ 0.01) and the difference in growth in experimental (with Ag NPs) and control conditions (blank growth media) compared to that of the wild-type strain more than 0.2 absorbance units.

The sensitivity of all of the initial "hit" mutant strains to each of the silver species was further confirmed by determining the IC_{50} for each strain. Specifically, a growth inhibition test was performed using a series of at least 8 concentrations of each Ag NP or ionic silver. To ensure against false negatives when comparing the results for different toxins, the IC_{50} value for each of the silver species was determined for all mutant strains that had come up as an initial hit in the screen in any of the toxins tested herein or had come up as an initial hit in the data set that we had previously reported for a cationic non-silver nanoparticle, PS-NH_2.[23] Again, each experiment was performed in at least quadruplicate to allow us to assess the reproducibility of the results reported herein. The IC_{50} with 95% confidence intervals for each candidate sensitive strain was calculated using nonlinear fit of log-normal distribution in the DRC package within the statistical software R. If the higher bound of the IC_{50} 95% CI was higher than the lower bound of the 95% CI of the IC_{50} for the wild-type strain, then the mutant strain was considered to be a *confirmed*, statistically significantly, sensitive strain. For clarity, the IC_{50} value of the *E. coli* wild-type (nonmutated) strain was set to 100%, and the IC_{50} values of the mutant strains were expressed as a percent of the sensitivity of the nonmutated strain.

Functional Classification and Clustering of Genes Responsible for Nanoparticle-Sensitive Phenotypes. The functions of the genes that were absent in mutants sensitive for certain Ag NP or $AgNO_3$ were analyzed using Ecocyc database (www.ecocyc.org), and the DAVID database (http://david.abcc.ncifcrf.gov/)[46] was used to reveal functional relationships between these genes. The genes whose absence resulted in bacterial sensitivity for the tested Ag formulations were clustered using self-organizing map clustering.[45] For clustering analysis, only those IC_{50} values of the mutants that were 10% less than the IC_{50} value of the nonmutated *E. coli* cells were included. Thus, any mutant that had an IC_{50} value of more than 10% lower than the nonmutated strain to any of the tested Ag formulation was added. Data for another positively charged nanoparticle, amino-functionalized 60 nm sized polystyrene (PS-NH_2), that was obtained in our previous study[23] were also included in the clustering analysis.

Imaging of Interactions between Ag NPs and Bacterial Cells by Microscopy. Atomic force microscopy was used to visualize the contact between the Ag NPs and the bacterial cells. Bacteria were grown in LB with 25 μg/mL of kanamycin at 37 °C to mid-log phase ($OD_{600} \sim 0.6$) and washed three times with DI water. The cells were exposed to IC_{10} concentrations of Ag NPs suspended in DI water for 30 min at room temperature and washed two times with DI water (each wash cycle involved: centrifugation at 2300*g*, removal of supernatant, and addition of equal amount of DI water). Ten microliters of each sample was pipetted onto freshly cleaved muscovite mica (TedPella, CA, USA). Ag NPs without bacterial cells were analyzed as abiotic control. The samples were allowed to evaporate prior to imaging. A Dimension 5000 instrument (Bruker, MA, USA) in tapping mode with a PPP-FM cantilever from Nanosensors (Nanoworld AG, Switzerland) was used to perform the imaging.

To prepare samples to visualize the cellular deformation by Ag NPs using transmission electron microscopy (TEM), bacterial cells were grown in 10 mL of bacterial growth media with Ag NPs overnight at a concentration corresponding to the IC_{10}. The cells were centrifuged (10 000*g*, 1 min) and fixed using 2.5% glutaraldehyde and formaldehyde for 2 h at room temperature, washed in PBS buffer, and stained with a solution of 1% OsO_4. Samples were washed with sodium acetate buffer (pH 5.5), additionally stained in 0.5% uranyl acetate for 12 h at 4 °C, dehydrated with ethanol (50−100%) for 10 min, and embedded in an Epon 812 resin. An ultramicrotome (RMC MTX) was used to cut 30 nm thick slices which were deposited on single-hole Formvar-coated grids. The grids were double-stained in 8% uranyl acetate solution for 25 min at 60 °C followed by lead citrate for 3 min at room temperature and then imaged using a JEOL 100CX TEM instrument.

ζ-Potential Measurements. For ζ-potential measurements, bacterial cells were grown and washed as described above for the preparation of cells for AFM measurements. One set of bacterial cells was used as negative control, and a second set was mixed with 0−16 μg/mL of Ag NPs suspended in DI water. The ζ-potential of cells ± NPs was measured by Zeta Pals ζ-potential analyzer using as described above.

Safe Handling of Nanomaterials. Nanoparticles as dry powders be handled in a chemical fume hood or powder enclosure or manipulated while the researcher is wearing a N95 filter mask. After suspension in aqueous solutions, standard good chemical hygiene practices should be employed. Sonication can result in aerolization and should only be performed on solutions that are in closed containers. More detailed recommendations are available in the *Nanotoolkit* developed by the *California Nanosafety Consortium of Higher Education* which is available online at http://www.cein.ucla.edu/new/p155.php.

Conflict of Interest: The authors declare no competing financial interest.

Acknowledgment. This study was performed in the University of California Center for Environmental Implications of Nanotechnology except for the syntheses of the Ag-BPEI and Ag-PVP NPs, which were performed in the Dept. of Environmental Engineering at the University of Cincinnati. We wish to

acknowledge the Nano and Pico Characterization lab of the California Nanosystems Institute, the Electron Microscope Services Center of Brain Research Institute, and the Molecular Shared Screening Resource at the University of California, Los Angeles. A.I. was supported by the ESF program Mobilitas; financial support from project SF0690063s08 of Estonian Ministry of Science and Education and EU project Nanovalid is acknowledged. This material is based upon work supported by the University of California Center for Environmental Implications of Nanotechnology in a grant from the National Science Foundation and the Environmental Protection Agency under Cooperative Agreement Number DBI-0830117. The paper has not been subjected to the U.S. Environmental Protection Agency's internal review, therefore, the opinions expressed in this paper are those of the author(s) and do not, necessarily, reflect the official positions and policies of the USEPA.

Supporting Information Available: Additional details for materials and methods related to determination of dissolved silver using atomic absorption spectroscopy and statistical analysis used to determine initial hits in high-throughput screen. Detailed information about physical characteristics of the Ag NPs studied herein (Figure S1), UV−vis spectra of the Ag NPs studied herein immediately after dispersion and after 24 h (Figure S2), induction of bacterial Ag^+ sensor with Ag NPs and $AgNO_3$ (Figure S3), growth of *E. coli* in the presence of coatings used for the production of Ag NPs (Figure S4), correlation between bacterial toxicity and ζ-potential of Ag NPs (Figure S5), electrophoretic mobility (ζ-potential) of *E. coli* cells and Ag NPs (Figure S6), TEM visualization of *E. coli* cellular changes in response to exposure to nanomaterials (Figure S7), results of statistical analysis of HTS data for Ag-BPEI and Ag-PVP demonstrated the high degree of reproducibility observed in these data (Figure S8), details of self-organizing map analysis of *E. coli* gene deletion strains that are more sensitive than the nonmutated *E. coli* strain to $AgNO_3$, Ag-cit_{10}, Ag-cit_{20}, Ag-PVP, and/or Ag-BPEI (Figure S9), clustering of genes responsible for bacterial sensitivity toward Ag and positively charged polystyrene nanoparticle, location of specific clusters on a self-organizing map (Figure S10). Tables of data: comparison of results for dissolved silver obtained using atomic absorption spectroscopy and UV−vis spectroscopy (Table S1), a list of *E. coli* mutant strains that were confirmed to be sensitive to Ag^+ ($AgNO_3$) and/or one or more of the Ag NPs; the IC_{50} values for each sensitive strain for Ag-cit_{10}, Ag-cit_{20}, Ag-PVP, Ag-BPEI, 60 nm PS-NH_2 NP (Table S2), clustering of gene deletion strains sensitive to $AgNO_3$, Ag-cit_{10}, Ag-cit_{20}, Ag-PVP, and/or Ag-BPEI strains as determined by self-organizing map (SOM) analysis (Table S3), correlations between overall responses derived from SOM analysis for Ag^+ ($AgNO_3$) Ag-cit_{10}, Ag-cit_{20}, Ag-PVP, Ag-BPEI, 60 nm PS-NH_2 NP (Table S4), grouping of gene deletion strains sensitive to each Ag formulation into functional clusters (Table S5). References for the Supporting Information are also included. This material is available free of charge *via* the Internet at http://pubs.acs.org.

REFERENCES AND NOTES

1. Nowack, B.; Krug, H. F.; Height, M. 120 Years of Nanosilver History: Implications for Policy Makers. *Environ. Sci. Technol.* **2011**, *45*, 1177–1183.
2. Marambio-Jones, C.; Hoek, E. A Review of the Antibacterial Effects of Silver Nanomaterials and Potential Implications for Human Health and the Environment. *J. Nanopart. Res.* **2010**, *12*, 1531–1551.
3. Tolaymat, T. M.; El Badawy, A. M.; Genaidy, A.; Scheckel, K. G.; Luxton, T. P.; Suidan, M. An Evidence-Based Environmental Perspective of Manufactured Silver Nanoparticle in Syntheses and Applications: A Systematic Review and Critical Appraisal of Peer-Reviewed Scientific Papers. *Sci. Total Environ.* **2010**, *408*, 999–1006.
4. Colman, B. P.; Arnaout, C. L.; Anciaux, S.; Gunsch, C. K.; Hochella, M. F., Jr.; Kim, B.; Lowry, G. V.; McGill, B. M.; Reinsch, B. C.; Richardson, C. J.; *et al.* Low Concentrations of Silver Nanoparticles in Biosolids Cause Adverse Ecosystem Responses under Realistic Field Scenario. *PLoS One* **2013**, *8*, e57189.
5. Nandakumar, R.; Espirito Santo, C.; Madayiputhiya, N.; Grass, G. Quantitative Proteomic Profiling of the *Escherichia coli* Response to Metallic Copper Surfaces. *Biometals* **2011**, *24*, 429–444.
6. Costanza, J.; El Badawy, A. M.; Tolaymat, T. M. Comment on "120 Years of Nanosilver History: Implications for Policy Makers". *Environ. Sci. Technol.* **2011**, *45*, 7591–7592.
7. Morones, J. R.; Elechiguerra, J. L.; Camacho, A.; Holt, K.; Kouri, J. B.; Ramírez, J. T.; Yacaman, M. J. The Bactericidal Effect of Silver Nanoparticles. *Nanotechnology* **2005**, *16*, 2346–2353.
8. Pal, S.; Tak, Y. K.; Song, J. M. Does the Antibacterial Activity of Silver Nanoparticles Depend on the Shape of the Nanoparticle? A Study of the Gram-Negative Bacterium *Escherichia coli*. *Appl. Environ. Microb.* **2007**, *73*, 1712–1720.
9. Carlson, C.; Hussain, S. M.; Schrand, A. M.; Braydich-Stolle, L.; Hess, K. L.; Jones, R. L.; Schlager, J. J. Unique Cellular Interaction of Silver Nanoparticles: Size-Dependent Generation of Reactive Oxygen Species. *J. Phys. Chem. B* **2008**, *112*, 13608–13619.
10. ElBadawy, A. M.; Luxton, T. P.; Silva, R. G.; Scheckel, K. G.; Suidan, M. T.; Tolaymat, T. M. Impact of Environmental Conditions (pH, Ionic Strength, and Electrolyte Type) on the Surface Charge and Aggregation of Silver Nanoparticles Suspensions. *Environ. Sci. Technol.* **2010**, *44*, 1260–1266.
11. ElBadawy, A. M.; Silva, R. G.; Morris, B.; Scheckel, K. G.; Suidan, M. T.; Tolaymat, T. M. Surface Charge-Dependent Toxicity of Silver Nanoparticles. *Environ. Sci. Technol.* **2011**, *45*, 283–287.
12. George, S.; Lin, S.; Ji, Z.; Thomas, C. R.; Li, L.; Mecklenburg, M.; Meng, H.; Wang, X.; Zhang, H.; Xia, T.; *et al.* Surface Defects on Plate-Shaped Silver Nanoparticles Contribute to Its Hazard Potential in a Fish Gill Cell Line and Zebrafish Embryos. *ACS Nano* **2012**, *6*, 3745–3759.
13. Hwang, E. T.; Lee, J. H.; Chae, Y. J.; Kim, Y. S.; Kim, B. C.; Sang, B.-I.; Gu, M. B. Analysis of the Toxic Mode of Action of Silver Nanoparticles Using Stress-Specific Bioluminescent Bacteria. *Small* **2008**, *4*, 746–750.
14. Smetana, A. B.; Klabunde, K. J.; Marchin, G. R.; Sorensen, C. M. Biocidal Activity of Nanocrystalline Silver Powders and Particles. *Langmuir* **2008**, *24*, 7457–7464.
15. Rai, M.; Yadav, A.; Gade, A. Silver Nanoparticles as a New Generation of Antimicrobials. *Biotechnol. Adv.* **2009**, *27*, 76–83.
16. Chernousova, S.; Epple, M. Silver as Antibacterial Agent: Ion, Nanoparticle, and Metal. *Angew. Chem., Int. Ed.* **2013**, *52*, 1636–1653.
17. Kittler, S.; Greulich, C.; Diendorf, J.; Köller, M.; Epple, M. Toxicity of Silver Nanoparticles Increases during Storage Because of Slow Dissolution under Release of Silver Ions. *Chem. Mater.* **2010**, *22*, 4548–4554.
18. Kim, J. S.; Kuk, E.; Yu, K. N.; Kim, J.-H.; Park, S. J.; Lee, H. J.; Kim, S. H.; Park, Y. K.; Park, Y. H.; Hwang, C.-Y.; *et al.* Antimicrobial Effects of Silver Nanoparticles. *Nanomed. Nanotechnol.* **2007**, *3*, 95–101.
19. Liau, S. Y.; Read, D. C.; Pugh, W. J.; Furr, J. R.; Russell, A. D. Interaction of Silver Nitrate with Readily Identifiable Groups: Relationship to the Antibacterial Action of Silver Ions. *Lett. Appl. Microbiol.* **1997**, *25*, 279–283.
20. Sondi, I.; Salopek-Sondi, B. Silver Nanoparticles as Antimicrobial Agent: A Case Study on *E. coli* as a Model for Gram-Negative Bacteria. *J. Colloid Interface Sci.* **2004**, *275*, 177–182.
21. Ruparelia, J. P.; Chatterjee, A. K.; Duttagupta, S. P.; Mukherji, S. Strain Specificity in Antimicrobial Activity of Silver and Copper Nanoparticles. *Acta Biomater.* **2008**, *4*, 707–716.
22. Xiu, Z.-M.; Zhang, Q.-B.; Puppala, H. L.; Colvin, V. L.; Alvarez, P. J. J. Negligible Particle-Specific Antibacterial Activity of Silver Nanoparticles. *Nano Lett.* **2012**, *12*, 4271–4275.
23. Ivask, A.; Suarez, E.; Patel, T.; Boren, D.; Ji, Z.; Holden, P.; Telesca, D.; Damoiseaux, R.; Bradley, K. A.; Godwin, H. Genome-Wide Bacterial Toxicity Screening Uncovers the Mechanisms of Toxicity of a Cationic Polystyrene Nanomaterial. *Environ. Sci. Technol.* **2011**, *46*, 2398–2405.

24. Baba, T.; Ara, T.; Hasegawa, M.; Takai, Y.; Okumura, Y.; Baba, M.; Datsenko, K. A.; Tomita, M.; Wanner, B. L.; Mori, H. Construction of *Escherichia coli* K-12 In-Frame, Single-Gene Knockout Mutants: The Keio Collection. *Mol. Syst. Biol.* **2006**, *2*, 2006.0008.
25. Tamae, C.; Liu, A.; Kim, K.; Sitz, D.; Hong, J.; Becket, E.; Bui, A.; Solaimani, P.; Tran, K. P.; Yang, H.; *et al.* Determination of Antibiotic Hypersensitivity among 4,000 Single-Gene-Knockout Mutants of *Escherichia coli*. *J. Bacteriol.* **2008**, *190*, 5981–5988.
26. Sharma, O.; Datsenko, K. A.; Ess, S. C.; Zhalnina, M. V.; Wanner, B. L.; Cramer, W. A. Genome-Wide Screens: Novel Mechanisms in Colicin Import and Cytotoxicity. *Mol. Microbiol.* **2009**, *73*, 571–585.
27. Becket, E.; Chen, F.; Tamae, C.; Miller, J. H. Determination of Hypersensitivity to Genotoxic Agents among *Escherichia coli* Single Gene Knockout Mutants. *DNA Repair* **2010**, *9*, 949–957.
28. Reyes, V. C.; Li, M.; Hoek, E. M. V.; Mahendra, S.; Damoiseaux, R. Genome-Wide Assessment in *Escherichia coli* Reveals Time-Dependent Nanotoxicity Paradigms. *ACS Nano* **2012**, *6*, 9402–9415.
29. Desai, K. K.; Miller, B. G. Recruitment of Genes and Enzymes Conferring Resistance to the Nonnatural Toxin Bromoacetate. *Proc. Natl. Acad. Sci. U.S.A.* **2010**, *107*, 17968–17973.
30. Nichols, R. J.; Sen, S.; Choo, Y. J.; Beltrao, P.; Zietek, M.; Chaba, R.; Lee, S.; Kazmierczak, K. M.; Lee, K. J.; Wong, A.; *et al.* Phenotypic Landscape of a Bacterial Cell. *Cell* **2011**, *144*, 143–156.
31. Monopoli, M. P.; Walczyk, D.; Campbell, A.; Elia, G.; Lynch, I.; Baldelli Bombelli, F.; Dawson, K. A. Physical−Chemical Aspects of Protein Corona: Relevance to *In Vitro* and *In Vivo* Biological Impacts of Nanoparticles. *J. Am. Chem. Soc.* **2011**, *133*, 2525–2534.
32. Zook, J.; Long, S.; Cleveland, D.; Geronimo, C.; MacCuspie, R. Measuring Silver Nanoparticle Dissolution in Complex Biological and Environmental Matrices Using UV−Visible Absorbance. *Anal. Bioanal. Chem.* **2011**, *401*, 1993–2002.
33. Liong, M.; France, B.; Bradley, K. A.; Zink, J. I. Antimicrobial Activity of Silver Nanocrystals Encapsulated in Mesoporous Silica Nanoparticles. *Adv. Mater.* **2009**, *21*, 1684–1689.
34. Käkinen, A.; Bondarenko, O.; Ivask, A.; Kahru, A. The Effect of Composition of Different Ecotoxicological Test Media on Free and Bioavailable Copper from $CuSO_4$ and CuO Nanoparticles: Comparative Evidence from a Cu-Selective Electrode and a Cu-Biosensor. *Sensors* **2011**, *11*, 10502–10521.
35. Li, M.; Zhu, L.; Lin, D. Toxicity of ZnO Nanoparticles to *Escherichia coli*: Mechanism and the Influence of Medium Components. *Environ. Sci. Technol.* **2011**, *45*, 1977–1983.
36. Gondikas, A. P.; Morris, A.; Reinsch, B. C.; Marinakos, S. M.; Lowry, G. V.; Hsu-Kim, H. Cysteine-Induced Modifications of Zero-Valent Silver Nanomaterials: Implications for Particle Surface Chemistry, Aggregation, Dissolution, and Silver Speciation. *Environ. Sci. Technol.* **2012**, *46*, 7037–7045.
37. Liu, J.; Sonshine, D. A.; Shervani, S.; Hurt, R. H. Controlled Release of Biologically Active Silver from Nanosilver Surfaces. *ACS Nano* **2010**, *4*, 6903–6913.
38. Ivask, A.; François, M.; Kahru, A.; Dubourguier, H.-C.; Virta, M.; Douay, F. Recombinant Luminescent Bacterial Sensors for the Measurement of Bioavailability of Cadmium and Lead in Soils Polluted by Metal Smelters. *Chemosphere* **2004**, *55*, 147–156.
39. Semple, K. T.; Doick, K. J.; Jones, K. C.; Burauel, P.; Craven, A.; Harms, H. Peer Reviewed: Defining Bioavailability and Bioaccessibility of Contaminated Soil and Sediment is Complicated. *Environ. Sci. Technol.* **2004**, *38*, 228A–231A.
40. Ivask, A.; Rõlova, T.; Kahru, A. A Suite of Recombinant Luminescent Bacterial Strains for the Quantification of Bioavailable Heavy Metals and Toxicity Testing. *BMC Biotechnol.* **2009**, *9*, 41.
41. Ivask, A.; Bondarenko, O.; Jepihhina, N.; Kahru, A. Profiling of the Reactive Oxygen Species-Related Ecotoxicity of CuO, ZnO, TiO_2, Silver and Fullerene Nanoparticles Using a Set of Recombinant Luminescent *Escherichia coli* Strains: Differentiating the Impact of Particles and Solubilised Metals. *Anal. Bioanal. Chem.* **2010**, *398*, 701–716.
42. Choi, O.; Hu, Z. Size Dependent and Reactive Oxygen Species Related Nanosilver Toxicity to Nitrifying Bacteria. *Environ. Sci. Technol.* **2008**, *42*, 4583–4588.
43. Khan, S. S.; Mukherjee, A.; Chandrasekaran, N. Studies on Interaction of Colloidal Silver Nanoparticles (SNPs) with Five Different Bacterial Species. *Colloids Surf. B* **2011**, *87*, 129–138.
44. McQuillan, J. S.; Infante, H. G.; Stokes, E.; Shaw, A. M. Silver Nanoparticle Enhanced Silver Ion Stress Response in *Escherichia coli* K12. *Nanotoxicology* **2012**, *6*, 857–866.
45. Rallo, R.; France, B.; Liu, R.; Nair, S.; George, S.; Damoiseaux, R.; Giralt, F.; Nel, A.; Bradley, K.; Cohen, Y. Self-Organizing Map Analysis of Toxicity-Related Cell Signaling Pathways for Metal and Metal Oxide Nanoparticles. *Environ. Sci. Technol.* **2011**, *45*, 1695–1702.
46. Dennis, G.; Sherman, B.; Hosack, D.; Yang, J.; Gao, W.; Lane, H. C.; Lempicki, R. DAVID: Database for Annotation, Visualization, and Integrated Discovery. *Genome Biol.* **2003**, *4*, P3.
47. Stoyanov, J. V.; Hobman, J. L.; Brown, N. L. CueR (Ybbl) of *Escherichia coli* Is a MerR Family Regulator Controlling Expression of the Copper Exporter CopA. *Mol. Microbiol.* **2001**, *39*, 502–512.
48. Solioz, M. Bacterial Copper Transport. In *Microbial Transport Systems*; Winkelmann, G., Ed.; Wiley-VCH Verlag GmbH&Co: Weinheim, Germany, 2002; p 361.
49. Jung, W. K.; Koo, H. C.; Kim, K. W.; Shin, S.; Kim, S. H.; Park, Y. H. Antibacterial Activity and Mechanism of Action of the Silver Ion in *Staphylococcus aureus* and *Escherichia coli*. *Appl. Environ. Microbiol.* **2008**, *74*, 2171–2178.
50. Klena, J. D.; Ashford, R. S.; Schnaitman, C. A. Role of *Escherichia coli* K-12 *rfa* Genes and the *rfp* Gene of *Shigella dysenteriae* 1 in Generation of Lipopolysaccharide Core Heterogeneity and Attachment of O Antigen. *J. Bacteriol.* **1992**, *174*, 7297–7307.
51. Papo, N.; Shai, Y. A Molecular Mechanism for Lipopolysaccharide Protection of Gram-Negative Bacteria from Antimicrobial Peptides. *J. Biol. Chem.* **2005**, *280*, 10378–10387.
52. Rosenfeld, Y.; Shai, Y. Lipopolysaccharide (Endotoxin)−Host Defense Antibacterial Peptides Interactions: Role in Bacterial Resistance and Prevention of Sepsis. *Biochim. Biophys. Acta* **2006**, *1758*, 1513–1522.